International Journal of Cardiac Imaging **9**: 201–212, 1993.

Experimental validation of a new quantitative method for the analysis of infarct size by cardiac perfusion tomography (SPECT)

Luc Mortelmans,[1] Johan Nuyts,[1] Johan Vanhaecke,[2] Alfons Verbruggen,[3] Michel De Roo,[1] Hilaire De Geest[2], Paul Svetens[4] & Frans Van de Werf[2]

[1] *Department of Nuclear Medicine,* [2] *Department of Cardiology,* [3] *Laboratory of Radiopharmaceutical Chemistry, University Hospital Gasthuisberg, Herestraat 49, B-3000 Leuven;* [4] *ESAT Department of Electrical Engineering, K.U. Leuven, Belgium*

Accepted 14 January 1993

Key words: infarct size, myocardial perfusion tomography, segmentation, SPECT, sestamibi

Abstract

Using global constraints and dynamic programming, a new model-based segmentation algorithm was developed to determine myocardial borders and basal plane. The segmented image is transformed to a countrate polar map and the infarct size (I.S.) is determined by comparison with a reference polar map. In order to evaluate our method the algorithm was applied to heart phantoms, to software simulations and to animal studies. In the last experiments, Tc-99m Sestamibi was used as a perfusion agent.

The total myocardial volume and infarct size of a Jasczack phantom were overestimated, especially when I.S. was expressed in absolute rather than relative values. It was proven by software simulations of cardiac Spect studies that those errors were mainly due to finite resolution effects causing a clear overestimation of myocardial thickness. Implementation of a constant thickness in the algorithm resulted in a much better correlation with actual values.

In a dog experiment the size of total myocardial volume of the area at risk during occlusion and of the final infarct size after thrombolysis was correlated with the histologic values obtained by planimetry after TTC staining. In 8 studies, an excellent correlation between the histologic area at risk versus the estimated perfusion defects was obtained ($r = 0.97$).

The automatic delineation of myocardial borders and valve plane was excellent even when perfusion defects were present. Manual intervention was only necessary in certain slices where a clear overlap between liver and myocardium was present in the dog studies. Segmental polar maps expressing count rate and volume information provided a visual and quantitative tool to evaluate the influence of thrombolysis in acute ligation experiments.

It is concluded that the new algorithm is ready to be used in a clinical environment for the quantitative evaluation of perfusion defects after acute myocardial infarction and for the follow-up of the therapeutic strategy.

Introduction

The extent of the area at risk, the amount of myocardial necrosis and the residual ventricular function are very important elements in assessing the results of thrombolytic therapy in acute myocardial infarction, in selecting the subsequent therapeutic (invasive versus conservative) strategy and in esti-

mating patients' prognosis [2]. Area at risk and infarct size can be evaluated by scintigraphic techniques. In our laboratory a new method for the quantification of perfusion defects on tomographic studies has been described previously [1]. The aim of this study was to evaluate this new technique by means of phantom measurement, artificial images and animal experiments.

In order to evaluate the quantitative performance of an algorithm, the obtained results have to be compared to the actual values. Therefore images of heart phantoms were carried out. The results of phantom studies suffer from many sources of error: attenuation, scatter radiation, limited collimator resolution, statistical noise, moderate adjustment of the gamma camera, etc. This makes the measurements reasonably representative for the clinical situation but precludes detailed analysis of each possible source of error separately. For these reasons simulated images were used as an alternative for heart phantoms with the following advantages:

- ideal phantoms can be generated so that results of the algorithm should be correct;
- the response of the algorithm to each of the error sources can be analyzed separately;
- images of any size, orientation and complexity can be generated.

This technique of simulated images is also used successfully by other authors [3, 4]. Eisner used his simulator to study various acquisition artifacts [3]. For that purpose they included a non-stationary point spread function. Nakajima used a simulator to study the effect of tracer clearance during acquisition [4].

The primary aim of the animal experiments was the comparison of scintigraphic infarct size (I.S.) and area at risk obtained by application of our delineation algorithm on Sestamibi perfusion images with histological I.S. and area at risk defined by triphenyltetrazolium (TTC) staining. Secondly, it was our intention to compare the area at risk after thrombotic occlusion of a coronary artery with the final infarct size by quantitative assessment of perfusion images acquired before and after thrombolysis.

Materials and methods

Phantom studies

Phantom measurements were performed with a Jaszczak heart phantom (model 7070, 7474, Data Spectrum Corporation, USA) placed in a perspex cylinder which simulates the body background. This phantom consists of a double cylindrical part connected to half a sphere simulating the ventricular wall. Cylinder (6440 ml with heart phantom included), myocardium (114.8 ml) and ventricular cavity (62.3 ml) can be filled with air, water or with a solution of a radioactive tracer. The length of the heart phantom is 7.45 cm; the radius is 4.90 cm and the thickness is 1.0 cm.

Inserts fixed in the wall of the heart phantom were used to simulate infarcts of different sizes and extent:

- an infarct parallel with the short axis planes with an extent of 90 degrees, a height of 2 cm and a volume of 5.8 ml;
- an infarct parallel with the short axis planes with an extent of 180 degrees, a height of 2 cm and a volume of 11.8 ml;
- an apical defect covering half of the apex with a volume of 15.3 ml;
- an apical infarct covering the whole apex with a volume of 32.5 ml. The first insert (5.8 ml) was placed in a superficial (s) and deep (d) position.

In our experiments the inserts contained no radioactivity as in the case of myocardial infarctions measured with perfusion tracers. The intraventricular cavity and the background cylinder were filled with air, water or a solution of Tc-99m. Based on patient data the ratio of radioactive concentration in the myocardium versus blood pool and background was 6 : 1 and 8 : 1, respectively. Thus, the ventricle, the blood pool and background contained 250, 23 and 1875 μCi of Tc-99m, respectively, corresponding to specific activities of 2.18; 0.37 and, 0.29 μCi/ml.

The acquisition was performed with a rectangular LFOV gamma camera (Technicare, Gemini 700) fitted with a high resolution collimator. Thirty-two projections with a matrix size of 64 × 64 and a zoom

factor of 1.6 were acquired over 180 degrees during 40 seconds per view. The longitudinal axis of the cylinder was parallel to the axis of rotation and to the surface of the examination bed. Slices of one pixel thick were reconstructed with a ramp filter without prefiltering to obtain maximum resolution.

Tests

The first tests concern the estimation of the total left ventricular mass by the new delineation algorithm. Twenty-eight measurements with a Jaszczak phantom were performed under various conditions: 13 of them with different types of infarct inserts and 15 without inserts. From the measurements without inserts, 7 were done with an empty cylinder, and 8 while the cylinder was filled with water. With infarcts, there were three groups: 5 measurements in air, 4 in water and 4 in a radioactive background solution. The actual volume of the myocardium is 115 ml. The pixel size was 5.1 mm so that one ml contained 7.5 voxels.

Measurements

The series of measurements without inserts in air, water and a radioactive solution was used as a reference database. A reference polar map was calculated by combining the studies in air and water separately so that the reference map was adapted to the attenuating medium of the experiment. A floating threshold (30, 40, 50, 60, 70, 80, 90%) of the local value of the polar map was used to define infarcted and normally perfused pixels. Five types of inserts were used as mentioned before.

Simulated images

A program was developed to create simulated heart images. In summary, this software package consists of three parts: Progen, Smooth and Poisson. In 'Progen' the user defines the type of the object. Based on the specifications a transverse slice through the object is created so that the radioactivity and the attenuation coefficient are known. For each slice a user specified number of projections is calculated taking into account the attenuation of the emitted radiation. The projections are computed by ray tracing using bilinear interpolation. The program 'Smooth' convolves the projection with a constant point spread function. This is an approximation since the point spread function in a projection image depends both on the distance from the source to the collimator and on the density of matter near the source. The point spread functions used are derived from line source measurements on a SPECT system. The routine 'Poisson' adds Poisson noise to the image. This noise is approximated by a Gaussian distribution with a standard deviation equal to the square root of the mean. Each projecton pixel is replaced by a random number that was generated according to the corresponding Gaussian distribution. The software was developed in-house. It is written in Pascal for Vax-VMS.

In the software experiments, the pixel size was set to 5.2 mm so that 1 ml contained 7.2 voxels. The point spread function had a full width at half maximum of 17 mm. The Poisson noise corresponds to a maximum intensity of 100 counts per projection pixel.

Determination of total volume

Corresponding to literature [5], the following dimensions for a standard left ventricle were used: length = 8.25 cm; width = 5.5 cm; thickness = 1.85 cm; myocardial mass = 150.3 ml; length to diameter ratio = 1.5. The same ratio of the radioactive concentrations was used as in previous section.

Software phantoms with varying dimensions have been generated and processed to evaluate the delineation algorithm:

- Six phantoms having the same height, diameter and shape but with different wall thickness, were produced. The thickness varied from 4.4 to 19 mm, covering a representative range of myocardial wall thickness.
- Eight left ventricles were simulated, all with a constant wall thickness of 1 cm and the same shape, but with a different size.

Determination of infarct size

The estimation of infarct size by means of a reference polar map was also evaluated on software phantoms. Five infarcts with the same shape and localization between apex and base but with different

size were generated. The studied volumes were: 1-4-11-22-36 ml, while the volume of the myocardium was 150 ml. Apex and base were intact. An average count rate and volume polar map were generated from five software phantoms with the same thickness and volume but varying length to width ratio. Several floating threshold values were applied to separate normal and infarcted pixels in the count rate polar map. The corresponding pixel volumes in the volume bull's-eye were added together to obtain infarct size.

Animal experiments

Description of the procedure

Seven mongrel dogs, four of which underwent the whole procedure, were premedicated with Hypnorm^R (10 mg Fluanisone/0.2 mg fentanyl pro ml, Duphar), 0.25 ml/kg intramuscularly and anaesthetized with sodium pentobarbital 15 mg/kg intravenously. Additional doses of pentobarbital were administered as required to maintain anaesthesia.

The dogs underwent three imaging sessions: a control session, a post infarction session, and a post thrombolysis section.

Control session. After anaesthesia, the dogs were injected with 15–20 mCi of Tc-99m MIBI followed by a tomographic acquisition one hour later.

Post infarct session. Two days later, a copper coil attached to a guide wire was advanced under fluoroscopic control via the carotid artery into the left anterior descendens coronary artery (LAD). The formation of an occlusive thrombus took 5 to 10 minutes and was confirmed by coronary angiography and was followed one hour later by an injection of 15–20 mCi of Tc-99m MIBI in a peripheral vein. Ten minutes after the injection, reperfusion was achieved by coronary thrombolysis using an intravenous infusion of rt-PA (10 $\mu g/kg^{-1}. min^{-1}$) followed by 2 X 1000 U heparine. After 20 minutes the infusion was stopped, the patency was documented by coronary angiography. Myocardial scintigraphy was performed after stabilization of the heart rhythm.

Post thrombolysis session. Another two days later, the dogs were injected again with the same dose of Tc-99m MIBI and tomographic acquistion was repeated 1 hour later. The patency of the LAD was confirmed by repeat coronary angiogram and then the hearts were arrested with potassium chloride intravenously and excised for *in vitro* evaluation of infarct size. The slices obtained for this purpose were put on the surface of a gamma camera and planar images were acquired. By this method, actual tracer distribution in the isolated cuts could be compared to the tracer uptake in the reconstructed tomographic slices.

In vitro *measurement of infarct size (dye perfusion and fixation technique followed by planimetry)*

Both right and left coronary ostia were cannulated as well as the LAD distal to the site of previous occlusion. The LAD was perfused with Ringer solution while the ostia were perfused at the same pressure with a mixture of Ringer solution and Evans blue. Two minutes later the LAD perfusion was switched to a triphenyltetrazoliumchloride (TTC) solution at 37° C for 10 minutes. Finally, the heart was fixed by perfusing the LAD area for another 5 minutes with 2% glutaraldehyde and both coronary ostia with a mixture of 2% glutaraldehyde and Evans blue.

After removing the right ventricle, the atria and the valve structures, the isolated left ventricle was cut in 1 cm thick slices perpendicular to the long axis. As a result of the above described dye perfusion technique, myocardium supplied by non-occluded coronary arteries colored blue, while in the occluded bed viable tissue stained brick red and infarcted tissue white.

Using calibrated color pictures of these slices, the left ventricular ring, the perfusion area of the LAD and the infarcted area were reproduced with black ink on a transparent plastic sheet.

Total left ventricular area, LAD perfusion area and infarcted area were calculated from data obtained by planimetry, performed on the black ink reproductions of the original color pictures, using a Quantimet 900 image analyzer (Cambridge Instruments, Ltd., Cambridge, England).

Scintigraphic acquisition and processing

The dogs were placed in the right lateral decubitus position on the acquisition table. Radioactive markers were acquired to obtain the same position in each session. Tomographic and planar imaging was performed with a large field of view camera (Technicare, Gemini 700) provided with a high resolution collimator and connected to a dedicated computer system (General Electric – Star II). During a circular orbit, sixty-four projections of thirty seconds were acquired using a 64×64 matrix and a zoom factor of two. The data were transferred to a VAX station for deconvolution of the projections with a Metz filter and reconstruction by a filtered back projection method. The transaxial slices were processed by our delineation technique.

For each dog, the first study was used to construct its own reference polar map. Several floating thresholds (0.2; 0.3. . .0.8) were used to delineate hypoperfused tissue. In the second session 'the area at risk' after acute thrombosis and before thrombolysis was obtained and in the third session the residual necrotic area after thrombolysis was calculated.

Quantitative assessment of left myocardial volume and infarct size

Our method, used to calculate the extent of hypoperfusion from SPECT images, is extensively described in a previous article [1]. Basically, this technique consists of four steps. First, 16 radial slices all through the long axis of the left ventricle are calculated instead of the conventional short axis slices. Next, the myocardial wall is delineated in each of the radial slices using a minimum costpath algorithm and an elliptic model. Then the valve plane is determined by an iterative fitting procedure. Finally a count rate and volume bull's-eye are computed. The delineation method uses dynamic programming in combination with a global shape model to delineate the endo- and epicardium and the basal plane. Based on this delineation, a polar map is calculated. Every pixel of the polar map corresponds to a small three-dimensional transmural region in the left ventricular wall. For every polar map pixel, the count rate, volume and wall thickness of the corresponding region are stored.

Perfusion defects are defined by comparing the polar map to a reference map. In order to do so, one of the maps should be normalized to the other. The normalization factor is determined in an iterative procedure. In each iteration the factor is chosen to minimize the squared differences between corresponding pixels in the two maps. After each iteration, however, all pixels with a difference larger than a threshold are discarded. The threshold is decreased after each iteration. As a result, the final normalization factor is determined by those regions of the polar maps that show sufficient similarity. Experience shows that perfusion defects are successfully discarded from the calculation of the normalization factor.

A count rate is considered abnormal if it is below a position dependent threshold. If a set of normal perfusion images is available, then a distribution of normal (relative) perfusion values can be calculated for every polar map pixel. This distribution reflects both the biological variability and the measurement inaccuracies. The threshold at every pixel is then defined as the mean value of the local distribution, minus a predefined number of standard deviations.

For the phantom studies, simulations and animal studies presented in this paper, such a set of normal perfusion studies is not available. In these cases, however, we do have an image which is free of defect (e.g. animal study prior to stenosis, phantom without inserts). Therefore, we defined the local threshold as a fraction of the (normalized) value of the same pixel in the defect-free polar map.

Results

Heart phantoms

The results of 28 calculations of the total myocardial volume in different attenuating media are presented in Fig. 1. The actual volume was 115 ml. The mean and standard deviation of the 18 values are respectively 146 ml and 6.5 ml.

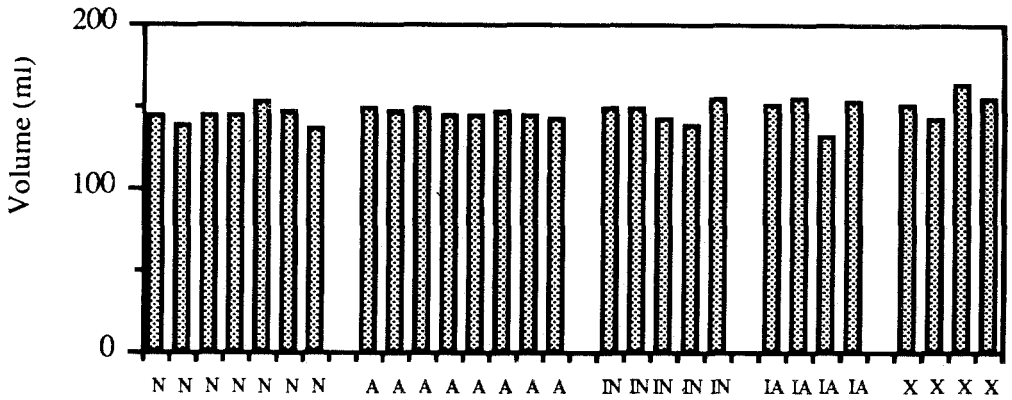

Fig. 1. Schematic presentation of measurements of total myocardial volume of a Jaszczack heart phantom (115 ml) fixed in a cylinder filled with air ('N' = no attenuation), water ('A' = attenuation) or a radioactive solution ('X' = attenuation and background). The calculations are carried out without and with inserts ('I'). Each bar presents one measurement. Inserts of 45°, 90°, 180° and covering the half or the whole apex were used. The volumes were determined after delineation of the myocardial borders and the valve plane with new software.

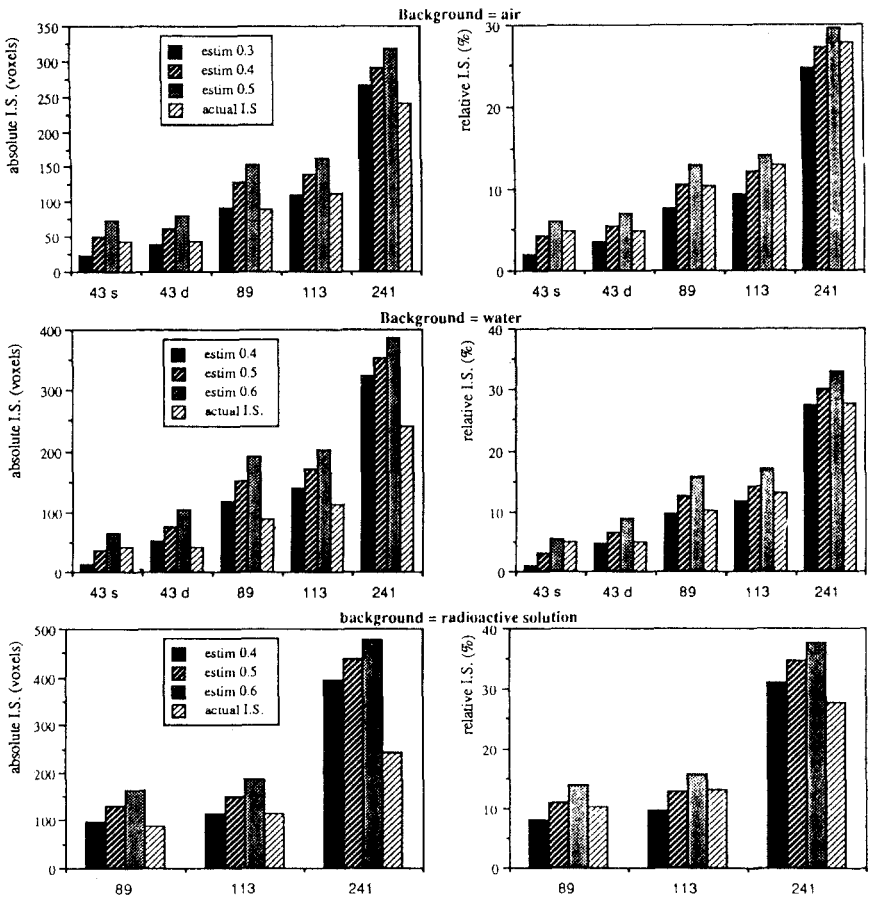

Fig. 2. Measurement of infarct size was carried out after positioning of five inserts with different size in the wall of a heart phantom: a superficial (43 voxels; 's') and deep infarction of 90° (43 voxels 'd'), an infarction of 180° (89 voxels), an infarction covering half the apex (113 voxels) and the whole apex (241 voxels). The heart phantom and the infarcted area were delineated with the new algorithm. Infarct volume was calculated by using floating thresholds on a reference polar map. *Upper row:* The experiments were performed in air. Floating thresholds of 0.3, 0.4 and 0.5 were used to calculate actual I.S. *Middle row:* Water was added as background medium. Floating thresholds of 0.4, 0.5 and 0.6 were used. *Left row:* Three inserts (infarction of 180°, the half and the whole apex) were used to evaluate infarct size determination in the case of a radioactive background. The same thresholds were used.

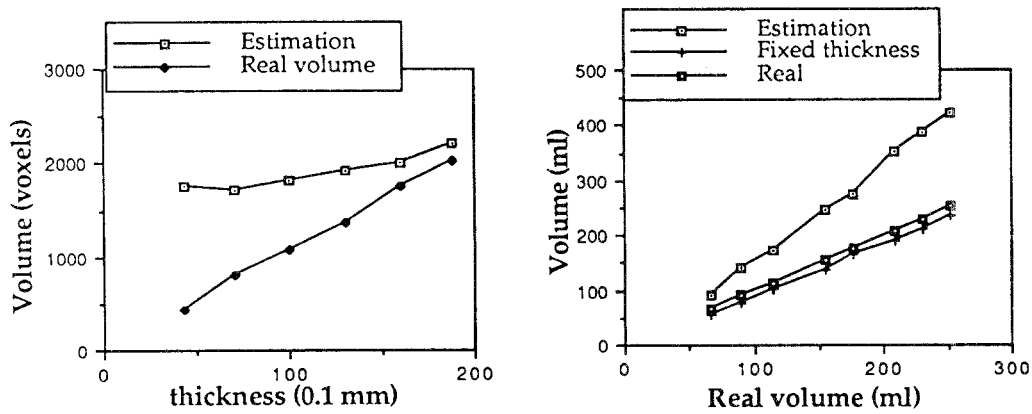

Fig. 3. Left side: determination of the total myocardial volume of software phantoms with varying thickness and constant weight, width and shape. The thickness varied between 4.4 and 19 mm. The real and estimated volume are indicated in voxels. The volumes were calculated with the new algorithm. *Right side:* determination of the total myocardial volume of software phantoms with a fixed thickness of 1 cm with increasing height and width. The volumes were also calculated when the delineation program was forced to produce contours with the exact thickness. Real volumes, estimated volumes and estimated volumes with fixed thickness were expressed in ml.

The results of absolute (voxels) and relative (% of total myocardium) infarct size are shown in Fig. 2. For both absolute and relative defect size, the best results, according to linear regression on the 13 measurements, were obtained for a threshold of 40%. For the absolute infarct size, we found an intercept of – 22 voxels, a slope of 1.47 and a regression coefficient r = 0.97. For the relative infarct size we found an intercept of – 1.8%, a slope of 1.08 and a regression coefficient r = 0.985.

Simulated images

Calculation of total volume

In a first series of experiments (Fig. 3 left side) the height, width and shape remained constant while the thickness varied from 4.4 mm to 19 mm. The phantoms were convolved with a point spread function of 17 mm FWHM and Poisson noise was added.

In a second series (Fig. 3 right side) the thickness was fixed at 10 mm while height and width of the phantom were gradually increased resulting in varying size and constant shape. To evaluate the positioning of the centerline lying just between the inner and outer border of the myocardium, the delineation program was also forced to produce contours with the exact thickness of 1 cm.

Calculation of infarct size

Results of the determination of infarct size by the application of three floating thresholds on a reference polar map are demonstrated in Fig. 4.

Animal experiments

With an injected dose of 15–20 mCi, a total of 15–20 Mcounts were obtained. The anterior hypoperfused zone of the second session was clearly demonstrated in all experiments. In two dogs the size of the hypoperfused area was nearly identical before and after thrombolysis and in the other two a clear decrease of hypoperfusion was found (Fig. 5). Contrary to patient studies, the apical slices were disturbed by overlap of the liver on the inferior wall due to breathing. A manual correction of the delineation algorithm was necessary in those regions be-

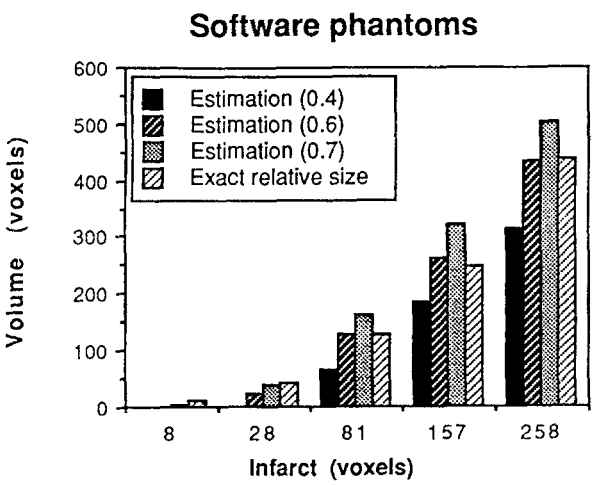

Fig. 4. Measurements of infarct size (8-28-81-157-258 voxels) while the whole myocardial volume was kept constant. The calculations were performed by application of three different floating thresholds (40-60-70%) on a reference polar map and compared to the correct value (software phantoms).

cause the liver overlapped intermittently perfused tissue. The partial irregular shape of the contour of the polar map can be explained by manual interaction.

The defect size was expressed as a percentage of the total myocardial volume of the myocardium. The values obtained with TTC staining are compared to the ones derived from the polar map analysis in Fig. 6, for three different floating threshold (40°, 50°, 60°). Combining the 8 measurements in a linear regression for every threshold, we obtained the following results for the intercept (– 90, – 89, – 12), for the slope (1.22, 1.38, 1.29) and for the correlation (0.94, 0.96, 0.97). With a threshold of 60% the difference between the scintigraphic 'area at risk' and the final 'infarct size' amounts to – 1%, 11%, 26% and 27%.

If we use a threshold of 50% because in reality the ideal threshold is not known, the following results were obtained from the four experiments: 1) the differences between the histologic I.S. (%) and the scintigraphic I.S. (%) were: – 7.9%, – 3.0%, 5.3%, 7.7%, respectively 2) the difference between the histological area at risk (%) measured as the perfusion territory of the occluded artery and the scintigraphic area at risk (%) were: – 0.7%, – 7.2%, 2.2%, – 4.0%.

In Fig. 7 the tracer distribution of a tomographic slice and of a planar post mortem image is compared to the picture of the stained myocardium and to its black ink reproduction.

Discussion

Estimation of total myocardial volume of a Jaszczak phantom was rather constant even when the measurements were performed in a (radioactive) attenuating medium and when inserts simulating infarcts were introduced. These data prove the stability and the reproducibility of our method. On the other hand, all results suffer from a clear overestimation of about 25%. This phenomenon is mainly caused by the finite resolution effect i.e. the structures that have to be resolved are smaller than the lower limit of detection of the gamma camera. The full width at half maximum of a line source measured in water at a distance from the collimator corresponding to the depth of the heart amounts to 15–17 mm for technetium and to about 20 mm for thallium. The thickness of the myocardial wall of the phantom is only 10 mm and, theoretically, cannot be resolved. If the thickness of the myocardial wall would increase, the estimation of the volume would progressively improve by a reduction of the finite resolution effect as is demonstrated with simulated images (Fig. 3 left side).

If the delineation algorithm was forced to produce contours with the correct thickness, even a small underestimation of the total volume was obtained (Fig. 3 right side). This effect can be explained by blurring of the myocardial image due to the limited resolution. Because of the convexity of the myocardium, blurring will produce a larger increase of background activity inside the myocardium versus outside. As a result, the centerline calculated by the program undergoes a slight shift of 2 to 3 mm. The overestimation of the myocardial thickness of 1 cm is far more important than the underestimation of the radius. Hence, the myocardial mass is systematically overestimated. When the

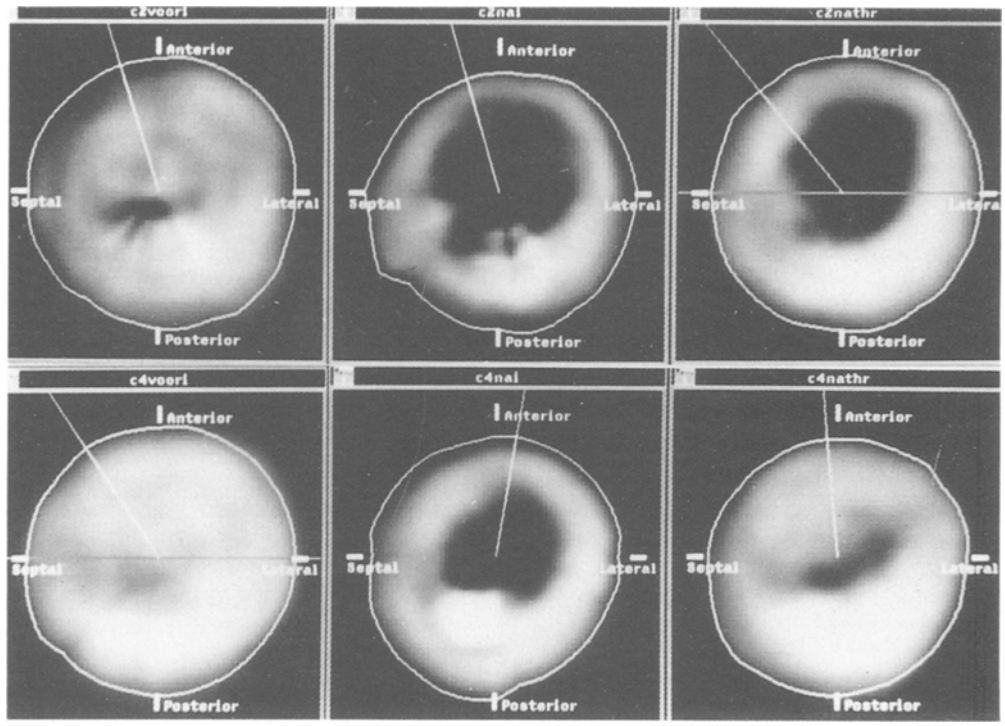

Fig. 5. Three polar maps (*left:* control; *middle:* after occlusion; *right:* after thrombolysis) of two animal experiments are shown. In the first case (upper level) no signs of reperfusion after thrombolysis were demonstrated, whereas a clear decrease of the defect after treatment was indicated in the other study (lower level). The hot spot in the middle picture (second experiment) is a part of the liver.

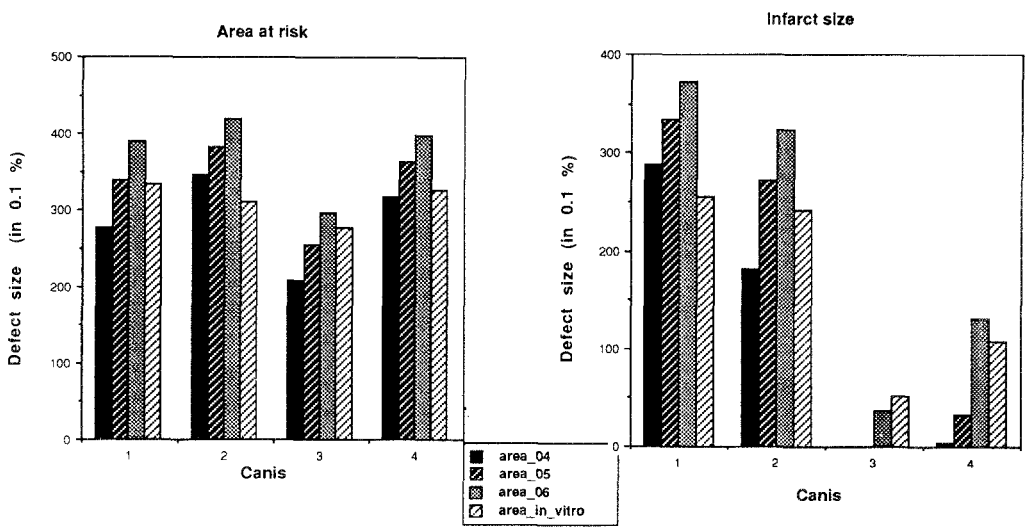

Fig. 6. Comparison of histologic area at risk and infarct size (I.S.) *in vitro* (black column) with tomographic area at risk and I.S. *in vivo* calculated with three floating thresholds (0.4, 0.5, 0.6) in four dogs ($C_{1\text{-}4}$). Both parameters are expressed in % of the whole myocardial volume.

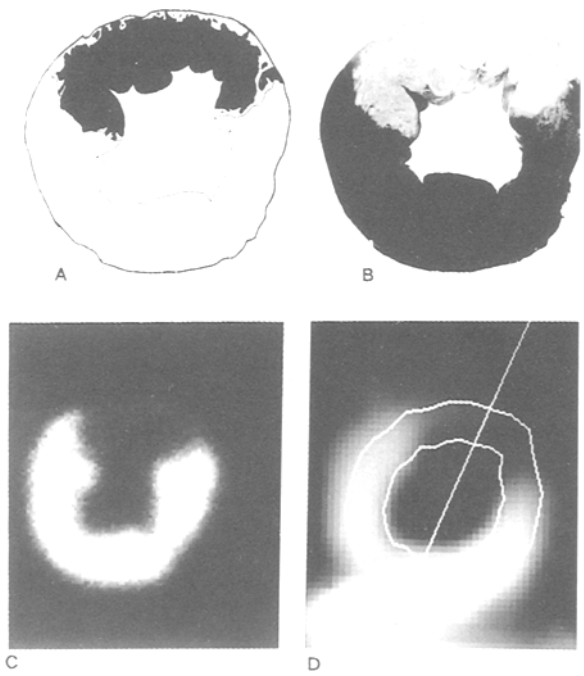

Fig. 7. Comparison of staining of myocardial tissue with the planar (*in vitro*) and tomographic (*in vivo*) distribution of Tc-99m MIBI in the same short-axis slice of an animal experiment. (*A*) Black ink reproduction of a TTC stained myocardial slice. Infarcted tissue is indicated in black ink. (*B*) Black and white picture of a transaxial myocardial slice. The black area corresponds to the perfusion territory of the nonoccluded vessel. In the occluded bed, the white area corresponds to necrotic tissue and the gray area to viable ischemic tissue. (*C*) Radioactivity distribution in a short-axis slice *in vitro*. The white area corresponds to perfused tissue while a large defect is shown in the anterior region. In the outer ring of this defect, some remaining tracer uptake is observed corresponding to the ischemic but viable tissue rim seen on the histological slices. (*D*) *Tomographic short-axis slice in vivo* of the same region. Perfused and nonperfused tissue is indicated by the edges defined by the delineation algorithm. Because of lower spatial resolution, the defect looks smaller and no residual tracer uptake is observed in this zone.

mass is increased with constant thickness, the underestimation of the radius decreases, resulting in a larger overestimation of the total mass.

For the same reasons as for the total volume (Fig. 2), an overestimation of absolute infarct size (voxels) was found and was more pronounced for apical infarcts because of delineation problems. As was demonstrated on the same figures, a relative measure of infarct size could partially solve this problem because the reference total mass was contaminated similarly by the finite resolution effect.

The optimal threshold for relative measurements had a constant value of about 0.4. The location of the smallest infarct (superficial or deep) did not influence the calculation of its size. The results of the measurements were not much influenced by the kind of background. For artificial images the best results were obtained with a threshold of 0.6 for the reference polar map. This difference in threshold between software and physical phantoms was due to the larger point spread function used with artificial images.

Estimates of infarct size agree better for artificial images than for physical phantoms (Fig. 4). The reason for this is probably that infarcts of the software phantoms all had the same shape and location, and differ in size only. On the contrary, the infarcts of the physical phantom were very different in shape and location since both apical and basal inserts were used.

The quality of the delineation and positioning of the valve plane was judged by visual inspection. In software phantoms, a good valve plane position (error < 1 pixel) was produced for basal infarcts up to 180° (half of the base).

For large apical infarcts, the estimated thickness of the invisible part of the myocardium was very sensitive to noise and to the exact shape of the perfused part of the myocardium. The use of a fixed realistic wall thickness can partially solve this problem. The already mentioned finite resolution effect is another reason for introduction of a fixed thickness especially in thallium SPECT studies. Therefore, a fixed value of 12 mm was used in the evaluation of clinical studies. The problem of finite resolution can be reduced in studies with new tracers such as Tc-99m Sestamibi, which have a better point spread function and produce higher count rates permitting gated acquisition. In principle, the situation is even better with positron emission tomographic studies which have a resolution value lower than the myocardial thickness, a better count rate and the possibility of gated acquistion [6].

The program only extracts information from the image, and does not correct for various errors due to scatter [7, 8] and attenuation [7, 9–11]. Deconvo-

lution can partially correct for scatter. Also motion of the heart caused by patient movements [12–14] and involuntary motion [15] may produce considerable errors. Finally, the beating of the heart causes blurring in ungated SPECT images and causes errors in the estimation of wall thickness [16]. Gating may overcome this error and may create possibilities for simultaneous analysis of wall motion [17]. To be quantitative, a clinical procedure should include corrections for all these errors. Fortunately, the use of a reference polar map of healthy volunteers implicitly corrects for some errors common to the patient's image and the reference images. Indeed, if both the reference bull's-eyes and the patient's bull's-eyes are degraded by similar amounts of attenuation and scatter, the effects of the degradation will be at least partially eliminated in a pixel-by-pixel comparison.

The possible use of Tc-99m Sestamibi for evaluation of thrombolytic therapy was proposed in animal and clinical experiments [18, 19]. Because Tc-99m Sestamibi does not leave the cells as Tl-201, it is feasible to inject a patient before thrombolytic therapy and to perform the acquisition a few hours later to evaluate the area at risk on admission. A second injection and scan, a few days later, permits the evaluation of the treatment. In two animals of this study a rather fixed perfusion defect and in the other animals a decrease of the perfusion defect was demonstrated. The polar maps, obtained by our delineation algorithm, appeared to be a very efficient and synoptic presentation of the temporal evolution of the perfusion defect. The quantitative processing of those maps will be a useful tool in the evaluation of therapy in individual patients or in large clinical trials.

As shown on the planar post mortem images, the tracer uptake in the heart is very similar to the distribution of normal, ischemic or necrotic tissue of the histologic slices. Even the outer rim of ischemic but viable tissue is faintly visible on the planar images. The *in vivo* tomographic slices designate the same areas of hypoperfusion but finer details have disappeared because of the low resolution. For this reason the distinction between ischemic and necrotic tissue in the same area was not possible.

It has to be stressed that a good correlation between histological I.S. and scintigraphic I.S. was found. In this context, it is important to note that a very large relative error on a very small infarct is clinically irrelevant but at the contrary, a small relative error on a large infarct might be clinically significant. Similar results were found when the histological area at risk was compared to the scintigraphic perfusion defect before thrombolysis. Comparable findings in animal experiments were reported for thallium-201 [20] and MIBI [19]. A long data acquisition time in comparison to the clearance of the tracer, as is the case for newer tracer as Tc-99m teboroxime, can be a significant cause of artifact. In this study using Tl-201 and Tc-99m Sestamibi, tracer clearance is negligible and a correction for radioactive decay was made. Our animal results obtained in real conditions of scatter radiation, noise, limited spatial resolution, etc., support the validation of our quantitative program.

We conclude that determination of infarct size by our new model-based and highly automated segmentation algorithm was successfully validated in experimental conditions and that it can be used in a clinical environment for the quantitative evaluation of perfusion defects.

Acknowledgements

We are gratefully indebted to Mrs. D. Schepers and Mrs. M.J. Vangoetsenhoven for their beautiful secretarial work, to Mrs. T. Stassen for the skillful animal preparation and to Mrs. V. Van den Maegdenbergh, Mr. P. Drent and Mr. E. Van de Gaer for the highly qualified technical work.

References

1. Nuyts J, Mortelmans L, Suetens P et al. Model-Based quantification of myocardial perfusion images. J Nucl Med 1989; 30: 1992–2001.
2. Geltman E, Abenschein D, Devries S. Assessment of coronary thrombolysis. Card Clin 1987; 5: 55–66.
3. Eisner R, Nowak D, Pettigrew R, Fajman W. Fundamentals of 180 degrees acquisiton and reconstruction in SPECT imaging. J Nucl Med 1986; 27: 1717–28.
4. Nakajima K, Shuke N, Taki J, Ichihara T, Motomura N, Bun-

ko H, Hisada K. A simulation of dynamic SPECT using radiopharmaceuticals with rapid clearance. J Nucl Med 1992; 33: 1200–6.
5. Eckner F, Brown B, Davidson D. Dimensions of normal human hearts. After standard fixation by controlled pressure coronary perfusion. Arch Path 1969; 88: 497–507.
6. Goldstein R, Mullani N, Wong W et al. Positron imaging of myocardial infarction with rubidium-82. J Nucl Med 1986; 27: 1824–9.
7. Chang W, Henkin R, Buddemeyer E. The sources of overestimation in the quantification by SPECT of uptakes in a myocardial phantom: Concise communication. J Nucl Med 1984; 25: 788–91.
8. Koral K, Wang X, Rogers W. SPECT compton-scattering correction by analysis of energy spectra. J Nucl Med 1988; 29: 195–202.
9. Hutton B, Bailey D, Fulton R. Estimates of left ventricular volumes by equilibrium radionuclide angiography: Importance of attenuation correction. J Nucl Med 1985; 26: 317–8.
10. Hosoba M, Wani H, Toyama H et al. Automated body contour detection in SPECT: Effect on quantitative studies. J Nucl Med 1986; 27: 1184–91.
11. Manglos S, Jaszczak R, Floyd C et al. Nonisotropic attenuation in SPECT: Phantom tests of quantitative effects and compensation techniques. J Nucl Med 1987; 28: 1584–91.
12. Eisner R, Noever T, Nowak D. Use of cross-correlation function to detect patient motion during SPECT imaging. J Nucl Med 1987; 28: 97–101.
13. Eisner R, Churchwell A, Noever T et al. Quantitative analysis of the tomographic thallium-201 myocardial bulls-eye display: Critical role of correcting for patient motion. J Nucl Med 1988; 29: 91–7.
14. Eisner R, Tamas M, Cedarholm J et al. Estimation of left ventricular mass from SPECT Tl-201: A new algorithm based on the 'bullseye' display validated in animal studies (abstract). J Nucl Med 1988; 29: 945.
15. Greckle W, Frank T, Links J et al. Correction for patient and organ movement in SPECT: Application to exercise thallium-201 cardiac imaging. J Nucl Med 1988; 29: 441–50.
16. Machac J, Howard L. Balk E et al. Computer modeling of planar myocardial perfusion imaging: Effect of heart rate and ejection fraction on wall thickness and chamber size. J Nucl Med 1986; 27: 653–9.
17. Barat J, Brendel A, Colle J et al. Quantitative analysis of left-ventricular function using gated single photon emission tomography. J Nucl Med 1984; 25: 1167–74.
18. Wackers F, Gibbons R, Verani M et al. Serial quantitative planar technetium-99m isonitrile imaging in acute myocardial infarction: Efficacy for non invasive assessment of thrombolytic therapy. JACC 1989; 14: 861–73.
19. Verani M, Jeroudi M, Mahmarian J et al. Quantification of myocardial infarction during coronary occlusion and myocardial salvage after reperfusion using cardiac imaging with technetium-99m hexakis 2-methyoxyisobutyl isonitrile. JACC 1989; 12: 1573–81.
20. Caldwell JH, Williams DL, Harp GD et al. Quantitation of size of relative myocardial perfusion defect by single-photon emission computed tomography. Circulation 1984; 70: 1048–56.